Theoretical and Applied Climatology (2019) 135:633–647
https://doi.org/10.1007/s00704-018-2393-9

ORIGINAL PAPER

The contrasting response of Hadley circulation to different meridional structure of sea surface temperature in CMIP5

Juan Feng[1] · Jianping Li[1,2] · Jianlei Zhu[3] · Yang Li[4] · Fei Li[5]

Received: 6 February 2017 / Accepted: 10 December 2017 / Published online: 13 February 2018

Abstract

The response of the Hadley circulation (HC) to the sea surface temperature (SST) is determined by the meridional structure of SST and varies according to the changing nature of this meridional structure. The capability of the models from the phase 5 of the Coupled Model Intercomparison Project (CMIP5) is utilized to represent the contrast response of the HC to different meridional SST structures. To evaluate the responses, the variations of HC and SST were linearly decomposed into two components: the equatorially asymmetric (HEA for HC, and SEA for SST) and equatorially symmetric (HES for HC, and SES for SST) components. The result shows that the climatological features of HC and tropical SST (including the spatial structures and amplitude) are reasonably simulated in all the models. However, the response contrast of HC to different SST meridional structures shows uncertainties among models. This may be due to the fact that the long-term temporal variabilities of HEA, HES, and SEA are limited reproduced in the models, although the spatial structures of their long-term variabilities are relatively reasonably simulated. These results indicate that the performance of the CMIP5 models to simulate long-term temporal variability of different meridional SST structures and related HC variations plays a fundamental role in the successful reproduction of the response of HC to different meridional SST structures.

1 Introduction

The Hadley circulation (HC) is mainly thermally driven, with its long-term variability closely related to the underlying thermal conditions. The relationship between the HC and underlying thermal conditions has been extensively explored using observations, such as sea surface temperature (SST). For example, Oort and Yienger (1996) reported that the HC is significantly correlated with the El Niño–Southern Oscillation (ENSO) phenomenon, i.e., a strengthening HC is seen during the El Niño events, and vice versa. However, it is reported that the relationship between the HC and ENSO events is insignificant in boreal winter and indicated that correlations vary markedly across different datasets (Mitas and Clement 2005, 2006). A similar result is reported in Tanaka et al. (2004). Later, Ma and Li (2007, 2008) further illustrated the relationship between the tropical SST and HC, and reported that interdecadal variations of the HC during boreal winters are closely related to SST anomalies over the Indo-Pacific warm pool (IPWP), and that interannual variations of the HC display a significant relationship with the SST over the eastern Pacific.

Electronic supplementary material The online version of this article (https://doi.org/10.1007/s00704-018-2393-9) contains supplementary material, which is available to authorized users.

✉ Jianping Li
ljp@bnu.edu.cn

[1] College of Global Change and Earth System Science, Beijing Normal University, Beijing 100875, China

[2] Laboratory for Regional Oceanography and Numerical Modeling, Qingdao National Laboratory for Marine Science and Technology, Qingdao 266237, China

[3] China-ASEAN Environmental Cooperation Center, Beijing, China

[4] College of Atmospheric Sciences, Chengdu University of Information Technology, Chengdu, China

[5] State key Laboratory of Atmospheric Boundary Layer Physics and Atmospheric Chemistry, Institute of Atmospheric Physics, Chinese Academy of Sciences, Beijing 100029, China

This indicates that ENSO contributes to the interannual variations of the HC. Feng et al. (2011) investigated the long-term variability of the boreal summer HC, and indicated that the interdecadal variability of boreal summer HC is related to the SST over the IPWP, whereas the interannual variations are related to the SST over the tropical eastern Pacific (Sun and Zhou 2014).

The relationship between the HC and SST has also been investigated using theoretical and numerical models. In particular, some earlier studies of simple theoretical models revealed the important impacts of SST on the HC. For instance, Lindzen and Nigam (1987) illustrated how boundary layer winds and vertical motion in the lower troposphere are influenced by the meridional inhomogeneous variations of SST via the alteration of the meridional SST gradient. Furthermore, it is found that the position of ascent and low-level convergence is influenced by the meridional structure of tropical SST through the adjustment of the atmospheric thermal structure and convergence process (Schneider and Lindzen 1977; Rind and Rossow 1984). Subsequent work supported this viewpoint and also indicated that the position of lower tropospheric convergence is sensitive to the meridional distribution of heating locations and profiles (Hou and Lindzen 1992). Subsequently, Clement (2006) used idealized climate model experiments to show that the transport of ocean heat plays an important role in determining the intensity and spatial structure of the seasonal HC. Chen et al. (2010) used an aqua-planet model to demonstrate that the HC intensifies in the deep tropics with low latitude warming. It was shown that the HC would weaken in most of the Intergovernmental Panel on Climate Change (IPCC) Fourth Assessment Report (AR4) coupled models under the warming scenarios (Vecchi and Soden 2007; Gastineau et al. 2008). The above research ascertains the important impacts of tropical SST on HC from the theoretical analysis and numerical models.

Recent observations have shown that the meridional structures of SST play a decisive role in determining the HC's long-term variability (Feng and Li 2013; Feng et al. 2013; Guo et al. 2016). For example, an equatorially symmetric SST structure is accompanied with an anomalous equatorially symmetric meridional circulation, and vice versa (Feng and Li 2013; Feng et al. 2015). And the variations of equatorially asymmetric SST contribute to the long-term variability of HC in the boreal summer and winter (Li and Feng 2017). To further establish the contrast responses of HC to different SST meridional structures, Feng et al. (2016) deconstructed the variations of the HC and SST into two components, i.e., the equatorially asymmetric (HEA for HC, SEA for SST) and equatorially symmetric (HES for HC, SES for SST) parts. They found that the responses of HEA to SEA are times to that of HES to SES within the period 1948–2013. This point is consistently observed in both observational and theoretical analysis. Consequently, the result explains why the dominant mode of seasonal HC's variability is equatorially asymmetric, for that a same magnitude variation in SST would induce larger anomalies in HEA than in HES. Therefore, the asymmetric–symmetric decomposition approach may provide us a feasible method to quantitatively evaluate whether the response of HC to tropical SST (including the involved physical process) in the GCCMs is reasonable.

Hu et al. (2013) evaluated the poleward expansion of the HC based on the Phase 5 of the Coupled Model Intercomparison Project (CMIP5). Feng et al. (2015) examined the capability of the CMIP5 models in capturing the HC's variability, and indicated that the reproduction of HC variation depend on the simulation ability of the meridional gradient of SST. However, few work assessing model simulations have been devoted to investigating the contrasting response of the HC to different SST meridional structures. Such research would useful for better cognizing the response of HC to tropical SST and the HC's variability, and could facilitate the ongoing improvement of the climate models. For example, a weakened (strengthened) of SES may associate with a corresponding variation in HES, implying the equatorially symmetric variation of HC would intensified (suppressed). Moreover, if the models can accurately reproduce the different responses of the HC to SST meridional structures, it would allow future variations of the HC to be detected.

The long-term simulations of CMIP5 have proved to be a helpful criterion for assessing model predictability and sensitivity with respect to SST forcing (Taylor et al. 2012). In the present study, we assess the performance of current coupled general circulation models (CGCMs) in simulating the responses of the HC to different SST meridional structures, and provide a comprehensive comparison of the differences in response among models and observations with the aim of improving the CGCMs.

The remainder of this manuscript is organized as follows. The models, observational datasets, and methodology used in this study are described in Section 2, and Section 3 outlines the capability of the CMIP5 models in reproducing the responses of the HC to different SST meridional structures in the observations and CMIP5 models. The potential causes of the model's simulation ability in reproducing the responses of HC to SST are investigated in Section 4. Finally, a discussion and our conclusions are presented in Section 5.

2 Models, observational datasets, and methodology

2.1 Models

The CMIP5 is a standard experimental protocol for the CGCMs and provides a community-based infrastructure in support of climate model intercomparison, validation, diagnosis, data access, and documentation. From the archive, we used outputs from 18 coupled models developed at different modeling centers (Table 1). Models were selected according to the model diversity

and data availability within period 1948–2004. The output data from the listed models had different horizontal and vertical resolutions. The physical processes involved differs between models; for example, some are Earth system models (e.g., CanESM2, BNU-ESM, etc.), which include biological processes. As the simulation periods in each model are different, model simulations of monthly mean SST and meridional wind within 1948–2004 were used. Notwithstanding, there are multiple outputs from most models, with different predictions derived solely from the initial conditions. Only the first simulations (i.e., r1i1p1) are analyzed in this study. We used historical simulations to assess the performance of the 18 models in simulating the responses of the HC to different SST meridional structures. For more details about the CMIP5 models, see http://cmip-pcmdi.llnl.gov/cmip5/availability.html.

2.2 Observational datasets

To validate the ability of the models in reproducing the responses of HC to different SST meridional structures, we used two atmospheric reanalysis datasets. The first was the National Centers for Environmental Prediction/National Center for Atmospheric Research (NCEP1) reanalysis that extends from the late 1940s to the present day and has a horizontal resolution of 2.5° × 2.5° (Kalnay et al. 1996). The second was the twentieth century reanalysis (20CR) dataset that extends from 1871 to 2010 and has a horizontal resolution of 2° × 2° (Compo et al. 2011). Two SST datasets used to examine the influence of tropical SST on the HC are version 1 of the Met Office Hadley Center Sea Ice and SST dataset (HadISST; Rayner et al. 2003), which has a 1° × 1° horizontal resolution, and the Improved Extended Reconstruction SST version 3b (ERSST; Smith et al. 2008) on a 2° × 2° horizontal resolution. According to the length of the model simulations, the period 1948 to 2004 was selected to evaluate the responses of the HC to different meridional structures of tropical SST. To show a direct comparison of the responses of the HC to different meridional SST structures, the seasonal diversities were not considered in this study. Additionally, as the HC is thermally driven, we examined only annual mean SSTs within the tropics.

2.3 Methodology

The HC is characterized by the mass stream function (MSF). It is obtained by vertically integrating the zonal mean meridional winds in the conventional way (Feng et al. 2013). Clockwise vertical circulation (the northern cell) is defined as positive

Table 1 Details of the CMIP5 models used in this study

Model name	Modeling center/country	Horizontal resolution (long × lat)	Vertical resolution (levels)	Reference
BCC-CSM1-1	Beijing Climate Center, China Meteorological Administration, China	2.81 × 2.77	17	Jiang et al. (2010)
BNU-ESM	Beijing Normal University, China	2.81 × 2.77	17	Ji et al. (2014)
CanESM2	Canadian Centre for Climate Modeling and Analysis, Canada	2.81 × 2.79	22	Chylek et al. (2011)
CCSM4	National Center for Atmospheric Research, USA	1.25 × 0.9	17	Gent et al. (2011)
CESM-CAM5	National Science Foundation, Department of Energy, NCAR, USA	1.25 × 0.9		Neale et al. (2012)
CNRM-CM5	Centre National de Recherches Meteorologiques, Meteo-France, France	1.41 × 1.40	17	Voldoire et al. (2013)
CSIRO-Mk3–6-0	Commonwealth Scientific and Industrial Research Organization (CSIRO), Australia	1.875 × 1.86	17	Collier et al. (2011)
EC-EARTH	European Centre for Medium-Range Weather Forecasts	1.125 × 1.125	16	Hazeleger et al. (2011)
FGOALs-g2	Institute of Atmospheric Physics, Chinese Academy of Sciences, China	2.81 × 1.67	17	Yu et al. (2011)
FIO-ESM	The First Institution of Oceanography, China	2.81 × 2.81	17	Qiao et al. (2013)
GFDL-ESM2M	NOAA Geophysical Fluid Dynamics Laboratory, USA	2.5 × 2.0	17	Dunne et al. (2013)
GISS-E2-H	National Aeronautics and Space Administration (NASA), USA	2.5 × 2.0	17	Schmidt et al. (2014)
HadCM3	Met Office Hadley Centre, UK	3.75 × 2.5	17	Gordon et al. (2000)
HadGEM2-ES	Met Office Hadley Centre, UK	1.875 × 1.25	17	Martin et al. (2011)
IPSL-CM5A-LR	Institut Pierre Simon Laplace, France	3.75 × 1.875	17	Dufresne et al. (2013)
MIROC-ESM	Atmosphere and Ocean Research Institute, National Institute for Environmental Studies and Japan Agency for Marine-Earth Science and Technology, Japan	2.81 × 1.77	23	Watanabe et al. (2011)
MPI-ESM-LR	Max Planck Institute for Meteorology, Germany	1.875 × 1.85	17	Giorgetta et al. (2013)
NorESM1-M	Norwegian Climate Centre	2.5 × 1.875	17	Bentsen et al. (2013)

and anti-clockwise vertical circulation (the southern cell) is defined as negative. That is, the sign of the MSF in the Southern Hemisphere is the opposite of that in the Northern Hemisphere. To determine the impacts of the meridional structure of SST on the HC, we linearly decomposed the variations of the HC and SST into two components: the equatorially asymmetric and equatorially symmetric components. According to Feng et al. (2016), the HES and HEA are defined as follows:

$$HES(j) = \frac{MSF(j) - MSF(-j)}{2}, \text{and } HEA(j) = \frac{MSF(j) + \mathrm{MSF}(-j)}{2}.$$

The SES and SEA are defined as:

$$SES(j) = \frac{SST(j) + \mathrm{SST}(-j)}{2}, \text{and } SEA(j) = \frac{SST(j) - \mathrm{SST}(-j)}{2},$$

where j and $-j$ are the meridional locations mirrored about the equator. Note that the sum of the equatorially asymmetric and symmetric components equals to the original variations of HC and SST. More details of the decomposition method are seen in Feng et al. (2017).

Empirical orthogonal function (EOF) analysis was used to detect the dominant mode of the equatorially asymmetric and symmetric components of the annual mean HC and zonal mean tropical SST. The annual cycle based on the period 1948–2002 of HC and SST is removed before performing the EOF, that is, the EOF modes as well as the corresponding principal components (PC) are based on the anomalies. The relationships between the principal modes and PC of the annual mean HEA and SEA, HES, and SES were investigated using spatial and temporal correlation analysis. The linear least squares regression is used to calculate the regression. The statistical significance of the correlation and regression values was assessed by means of a two-sided Student's t test. All of the CMIP5 historical simulations were linearly interpolated to the same horizontal resolution as the NCEP1 reanalysis for an objective comparison.

3 The responses of HC to different meridional structures of SST in observations and CMIP5 models

3.1 Simulated annual HEA, HES, SEA, and SES

First of all, the performance of the CMIP5 models in simulating the climatological spatial patterns of annual mean HEA, HES, SEA, and SES is examined. To quantitatively examine the accordance between the CMIP5 models and observations, a set of Taylor diagrams is employed to compare the model's performance based on the climatological distributions of HEA, HES, SEA, and SES (NCEP1 for HEA and HES, and ERSST for SEA and SES). Similar features are seen in the climatological HEA for all models, where they are centered at the equator with centers located in the lower troposphere, with an extent of approximately 60° latitude from the Southern Hemisphere to the Northern Hemisphere (Fig. A1). We see that the spatial structures of HEA between the models and observations are significantly correlated with each other, with correlation coefficients all beyond 0.8 (Fig. 1a). This result indicates that the CMIP5 models show well skills in capturing the climatological characteristics of HEA. For the simulated amplitude of the climatological HEA, evident biases are seen comparing with the observations. It shows a general amplitude underestimation of the HEA pattern in the models, with a smaller than 1.0 ratio of the standard deviation of the modeled to the observed HEA patterns, despite that some models, i.e., CSIRO-Mk3-6-0, MPI-ESM-LR, EC-EARTH, and MIROC-ESM, generate overestimates. Similarly, all models capture the spatial structure of HES, with the combined ascending branch located at the equator, and the cell extending from 30°S to 30°N (Fig. A2). This point is further observed from the high spatial correlation coefficients, with all of the coefficients being greater than 0.9. However, an overestimate of HES amplitude is seen in most models except CSIRO-Mk3-6-0 (Fig. 1b). This result indicates that the simulations of climatological HEA and HES are reasonable in the CMIP5 models.

In contrast to the results for HEA and HES, all the models underestimate the amplitude of SEA (Fig. A3), but with significant spatial correlations with the observation (Fig. 1c). As to the SES, it is seen that all of the models accurately depict the parabola-like variations of SES, with centers located at the equator and a maximum at around 5° latitude within each hemisphere (Fig. A4). This point is further verified from the high spatial correlations between the models and observations of SES, with coefficients all greater than 0.93. However, unlike to the SEA, a general overestimate of the SES's amplitude is seen (Fig. 1d).

In general, despite certain biases are exist in the amplitude, all of the models show satisfactory skills in depicting the fundamental characteristics of the equatorially asymmetric and symmetric components of HC and tropical SST. The simulations of the climatological spatial pattern of annual mean HEA, HES, SEA, and SES are consistent nicely with the observations. Meanwhile, the satisfactory performance of the models in reproducing the above spatial structures highlight the skills of the CMIP5 models, which provide the basic guarantee for further detecting their ability in reproducing the response of HC to different SST meridional structures.

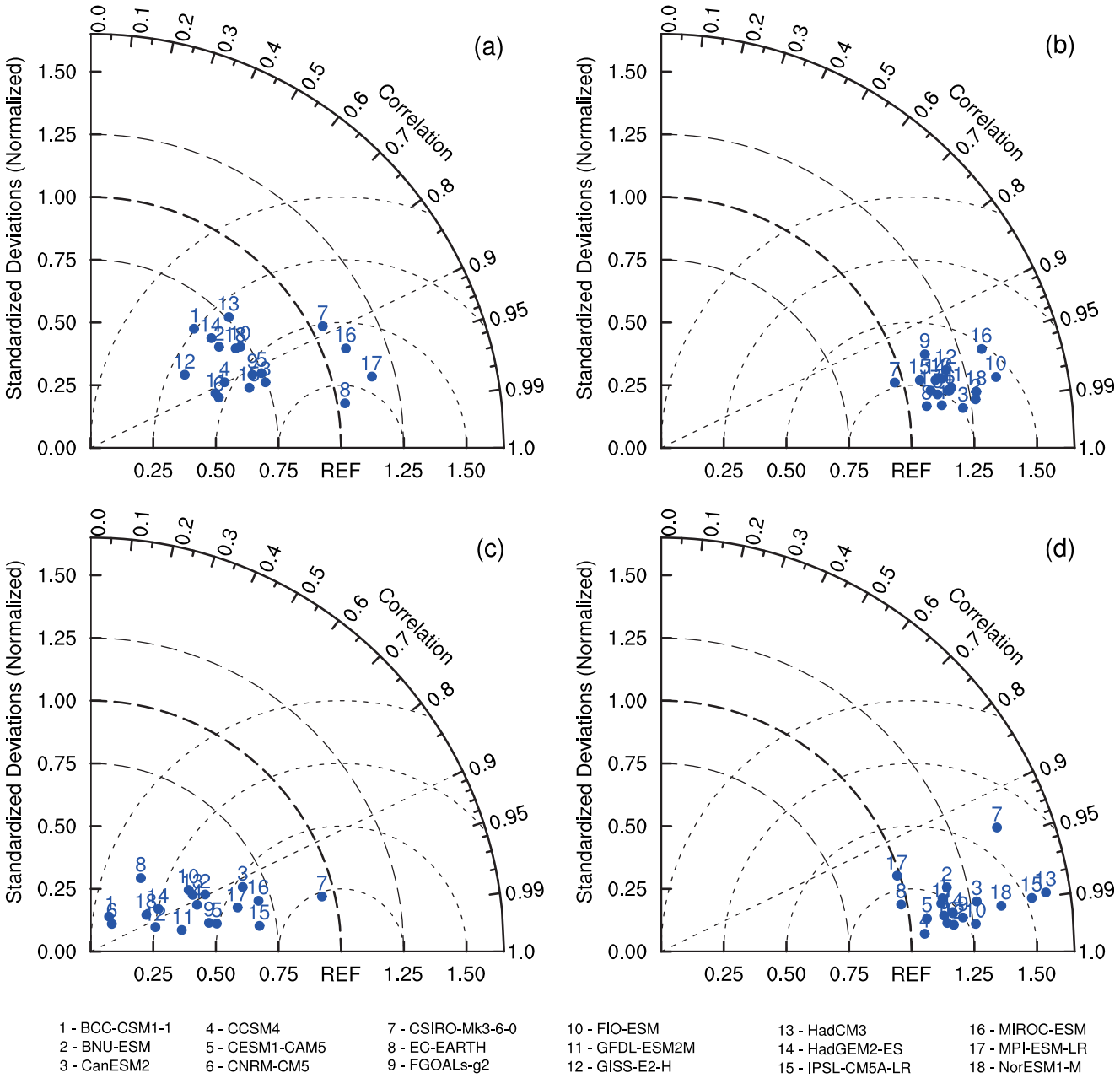

Fig. 1 Taylor diagram of the climatological distribution of **a** HEA, **b** HES, **c** SEA, and **d** SES. The correlation coefficients and ratio of the standard deviation between models and reanalysis data (NCEP1 and ERSST) are shown by the cosine of the azimuth angle and the radial distance, respectively. REF on the horizontal axis indicates the reference point (NCEP1 and ERSST)

3.2 Response ratio between HEA to SEA and HES to SES

Having discussed the ability of the CMIP5 models in reproducing the climatological structures of the equatorially asymmetric and symmetric components of the HC and zonal mean SST, in this section we compare the responses of HEA to SEA and HES to SES in both the observations and CMIP5 models. To quantitative assess the response of HC to different SST meridional structures, EOF is employed to obtain the principal variability of HEA, HES, SEA, and SES. According to Feng et al. (2016), the variation of HES is mainly associated with SES, and that the variability of HEA is linked to variations of SEA. The scatter plot of the first PC of HEA with respect to that of SEA as well as the HES to SES is shown in Fig. 2. It is seen that the response of HEA to SEA is ~ 7 times that of HES to SES in the observations in both the NCEP1 and 20CR reanalysis data with respect to different SST reanalyses. This

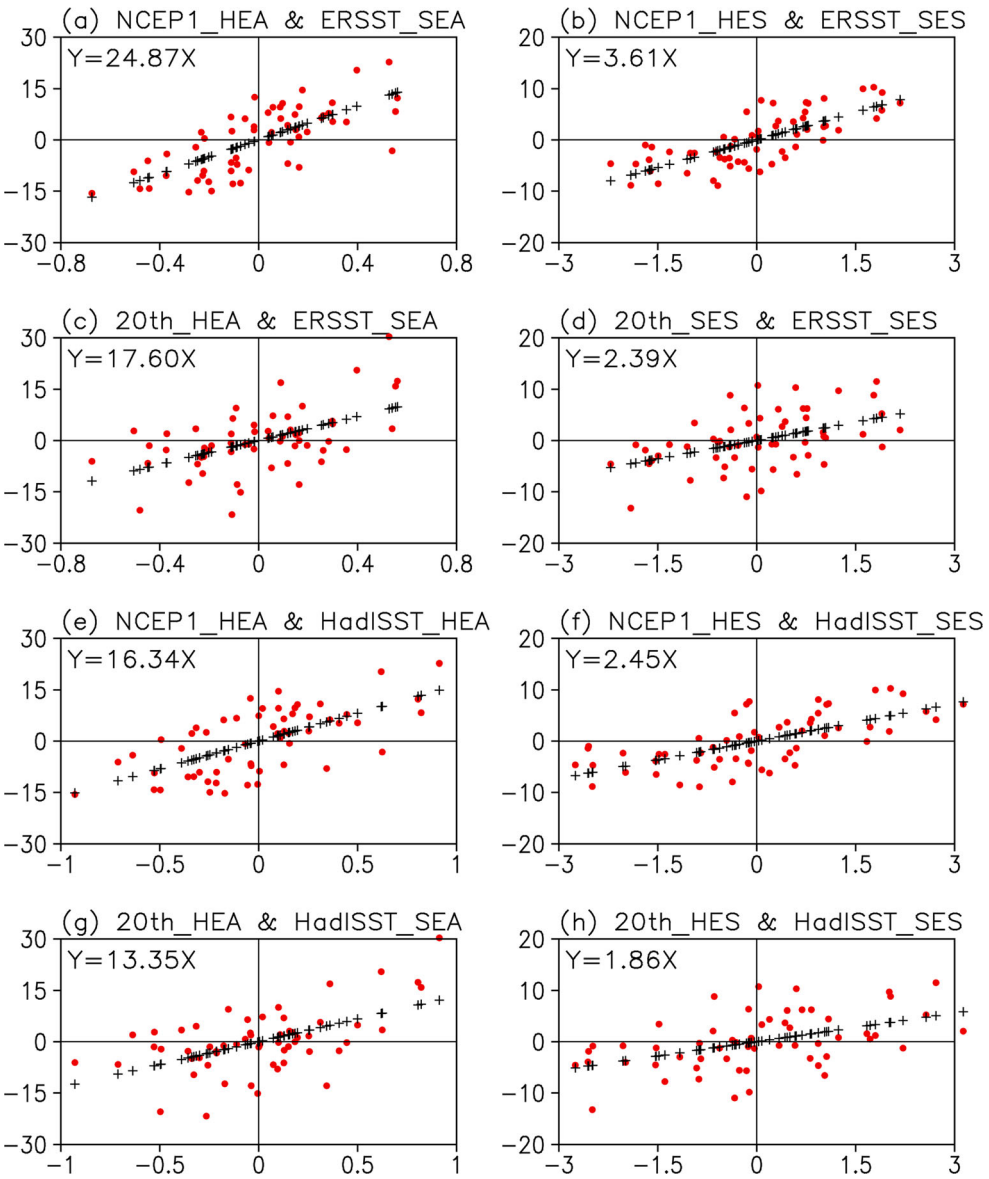

Fig. 2 Left panel, scatter plot of the first PC of the SEA against the first PC of the HEA based on different reanalyses. The red dots are the PCs of HEA and SEA (SES), the black dots are the linear fit of the scatter, for which the regression coefficient is shown. Right panel, as in the left, but for the scatter plot of the first PC of the SES against the first PC of the HES

suggests a contrasting response induced by the differences in the meridional structures of SST as reported in Feng et al. (2016). However, the response ratio between HEA to SEA and HES to SES in the CMIP5 models shows large uncertainties (Table 2). The BCC-ESM1-1, IPSL-CM5A-LR, and FGOALs-g2 models overestimate the responses ratio associated with different SST meridional structures. In contrast, CSIRO-Mk3-6-0, CCSM4, FIO-ESM, GISS-E2-H, and GFDL-ESM2M models underestimate the response differences. Moreover, it is seen that the response difference is simulated relatively well in the BNU-ESM, CanESM2, CNRM-CM5, HadGEMs-ES, and HadCM3 models. The above analysis indicates that the performance of the models in simulating the response contrast of HC to different tropical SST meridional structures differs among the individual models. Additionally, the exaggeration or underestimation of the asymmetric or symmetric components of HC or SST, or their combined impacts, could lead to inaccurate simulations of the different responses, and the potential causes will be discussed in the following.

4 Possible causes of the simulated response differences of HC to SST

The difficulty in understanding the response contrast of HEA to SEA with respect to HES to SES is that variations arising from HC and SST both could induce uncertainties in the response differences. In this section, both the spatial and temporal variations of long-term variability of HEA, HES, SEA,

Table 2 The response coefficients of HEA to SEA, HES to SES, and their ratio in the reanalysis data and CMIP5 models

Data types	HEA-SEA	HES-SES	Ratio
NCEP1-ERSST	24.87	3.61	6.9
NCEP1-HadISST	16.34	2.45	6.7
20CR-ERSST	17.60	2.39	7.4
20CR-HadISST	13.35	1.86	7.2
BCC-CSM1-1	19.83	0.27	74.6
BNU-ESM	26.03	3.30	7.9
CanESM2	18.26	2.15	8.5
CCSM4	8.73	3.21	2.7
CESM1-CAM5	2.20	−0.80	–
CNRM-CM5	15.63	2.13	7.3
CSIRO-Mk3-6-0	10.63	2.59	4.1
EC-EARTH	7.64	0.42	18.2
FGOALs-g2	13.74	0.68	20.4
FIO-ESM	18.21	3.93	4.6
GFDL-ESM2M	19.08	4.37	4.4
GISS-E2-H	12.72	3.39	3.7
HadCM3	17.36	3.05	5.7
HadGEM2-ES	15.29	2.27	6.7
IPSL-CM5A-LR	6.83	0.43	15.8
MIROC-ESM	12.33	1.12	11.0
MPI-ESM-LR	−0.95	2.11	–
NorESM1-M	14.99	2.78	5.4

and SES are detected to assess the ability of the CMIP5 models in reproducing the responses ratio. As discussed below, we see that the explained variances of the first dominant mode of year-to-year variability of HEA, HES, SEA, and SES are greater than 50%, indicating that the foremost variations could be explained by the first dominant mode. Thus, in the context below, only the first leading mode is analyzed.

4.1 Long-term variability of the HEA and HES

In the observation, the first principal mode of HEA is dominated by an equatorially asymmetric cell, and explains around 70% of the variance in the reanalyses. This mode centers on the equator and extends approximately 30° to the north and south, as is consistently observed in both the NCEP1 and 20CR data (Fig. 3a, b). We found that most of the models depict the spatial structure of this mode well in both spatial structure and amplitude, and accounts for a variance of about 70% (Fig. 4). A notable exception is the IPSL-CM5A-LR model, which shows a large departure from the observations, in which a broader extent and a smaller variance are observed, and the center deviates from the equator (Fig. 4o). Except the IPSL-CM5A-LR model, the principal mode of HEA accounts for most of the variation, which is further resolved by a high spatial correlation between the observations and models, with coefficients between 0.73 and 0.89 (figures not shown).

As to the leading mode of HES, an equatorially symmetric mode dominates the variability of HES and explains a variance of around 50%, with the combined ascending branch at the equator, and two descending branches located in the extra tropics in each hemisphere (Fig. 3c, d). The extent of this mode in NCEP1 is much broader than in 20CR, but the intensity of this mode in the two reanalyses is consistent. However, there are many uncertainties in the simulations of this mode determined from the CMIP5 models. The spatial structure, amplitude, and the explained variances (varying from 36.6 to 84.2%) show certain differences from the observations (Fig. 5). The spatial correlation of this mode between the observations and models varies from 0.32 to 0.56, apart from IPSL-CM5A-LR because of its limitation in capturing the spatial distribution. Our results indicate that although the climatological features of HES are better simulated in the CMIP5 models than those of HEA, the variabilities are better explained by the simulations of long-term HEA, which also compare well with the observations.

The simulations of the PCs of these modes of long-term variations of HEA and HES are further evaluated in Fig. 6. None of the correlation coefficients for the interannual variations of the PCs for HEA and HES between the observations and those from the models are significant. This implies that all of the models were not able to accurately simulate the temporal evolution of the first leading mode of the HEA and HES.

4.2 Long-term variability of SEA and SES

The leading mode of SEA is equatorially asymmetric, with the minimum in the Northern Hemisphere and the maximum in the Southern Hemisphere, and decreasing with latitude (Fig. 7a). This mode explains 90.2% of the variance in the ERSST data and 88.8% in the HadISST data. The long-term variability of SES is dominated by an equatorially symmetric structure (Fig. 7b), which explains 93.1% of the variance in the ERSST data and 92.0% in the HadISST data. Despite there being a little difference in the modes of SEA and SES between ERSST and HadISST, the spatial distribution of the dominant modes are consistent, and the explained variance is the same, implying the reliability of this mode. The close linkage between the HC and SST is further established by the high correlations of their corresponding PCs, with the correlation coefficients being greater than 0.7 for that of HEA and SEA, and HES and SES based on the NCEP1 and ERSST. Besides, it is seen that the variations of SES is closely linked with El Niño–Southern Oscillation (ENSO) in that both El Niño and La Niña are corresponding to equatorially symmetric SST anomalies (Zhang et al. 2009).

The simulations of the long-term variability of SEA and SES are displayed in Figs. 8 and 9, respectively. Most models,

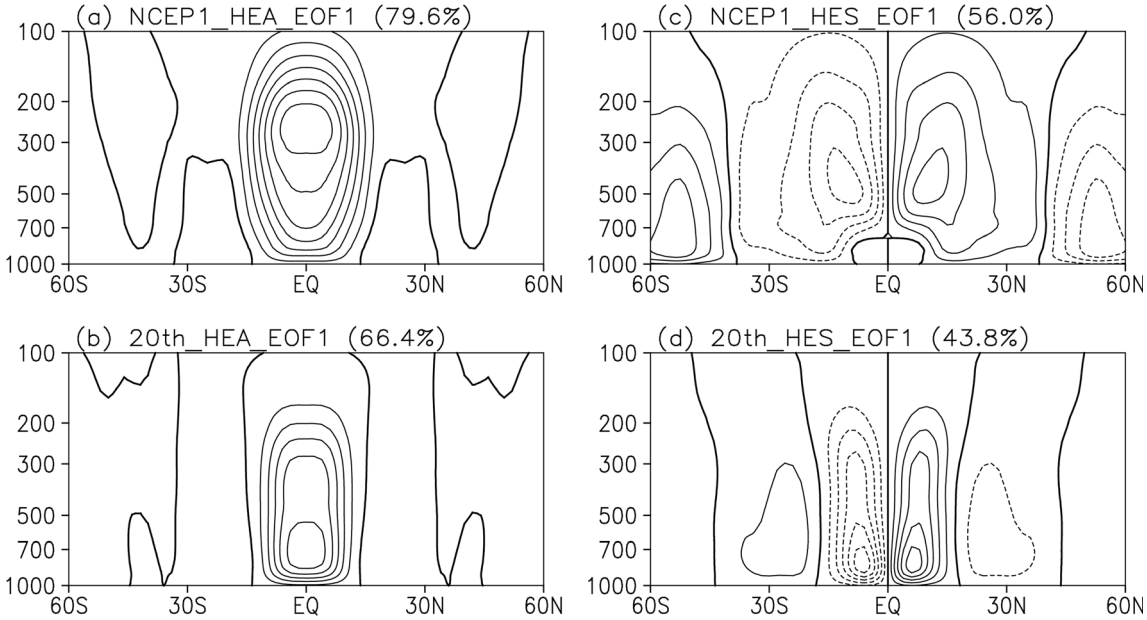

Fig. 3 **a** The first principal mode of HEA based on the NCEP1. The contour interval is 0.02 × 10^{10} kg/s. Positive (negative) contours are shown as solid (dotted) lines. **b** As in (**a**), but based on the twentieth-century reanalysis. **c** As in (**a**), but for the HES. **d** As in (**c**), but based on the twentieth-century reanalysis

except BNU-ESM, reproduce the spatial distribution of the long-term variability of SEA reasonably well. In addition, all models underestimate the explained variance of this model. However, for long-term variations of SES, the amplitudes of this mode vary markedly among the CMIP5 models despite the explained variance of this mode being similar to the observations. The amplitude in the MIROC-ESM, EC-EARTH, IPSL-CM5A-LR, BCC-CSM1-1, and FGOALs-g2 models are much smaller than seen in the observations. Meanwhile, large bias is seen in the simulated temporal long-term variability of SEA (i.e., PCs), apart from in GISS-E2-H (Fig. 6c). By contrast, most of the models were able to simulate the changing long-term variability of SES well, and this is reflected by the significant correlations in the PCs between observations and models (Fig. 6d).

Therefore, as discussed above, the larger response ratio of HEA to SEA with respect with HES to SES in models BCC-ESM1-1, FGOALs-g2, and IPSL-CM5A-LR may be due to the underestimated response of HES to SES. In contrast, the low response ratio in the GISS-E2-H, CCSM4, and CSIRO-Mk3-6-0 models may be caused by the underestimated response of HEA to SEA. Also, the low response ratio shown in FIO-ESM and GFDL-ESM2M models may be due to the exaggerated response of HES to SES. And as mentioned, although the long-term temporal variation for both the equatorially asymmetric and symmetric variations are not as well simulated as the spatial structures, the temporal variability of SES is relatively better depicted in the models, implying an improved performance in simulating the equatorially symmetric SST variations (Kug et al. 2012).

5 Discussion and conclusions

This study used historical simulations generated by 18 CMIP5 models to test their ability in simulating the response contrast of HC to different SST meridional structures. By linearly decomposing the variations of the HC and SST into two components, the equatorially asymmetric (i.e., HEA and SEA) and symmetric (i.e., HES and SES) variations, it is shown that the models show nice skills in simulating the spatial structures and amplitudes of the climatological HEA, HES, SEA, and SES. Moreover, the climatological characteristics of HES and SES show better simulation performance than those of HEA and SEA. Overall, the models showed reasonable capability in reproducing the climatological features of the equatorially symmetric components for both SST and the HC.

As to the long-term variability, we found that most models captured the spatial structures of the principal mode of HEA and HES well in both spatial distribution and amplitude. The IPSL-CM5A-LR model showed evident shortcomings in producing the spatial structure of the principal mode of HEA. Similarly, a limited ability in simulating the spatial distribution of the principal mode of HES was observed. On the other hand, the first dominant modes of SEA and SES were reproduced by the CMIP5 models. Although there are certain differences in the amplitudes and explained variances, the long-term variability of the spatial distribution of the principal modes was reproduced. With the exception of GISS-E2-H, we found that the models cannot reproduce the temporal variations of the corresponding PCs of HEA, HES, and SEA. In contrast, most of the models showed significant correlations

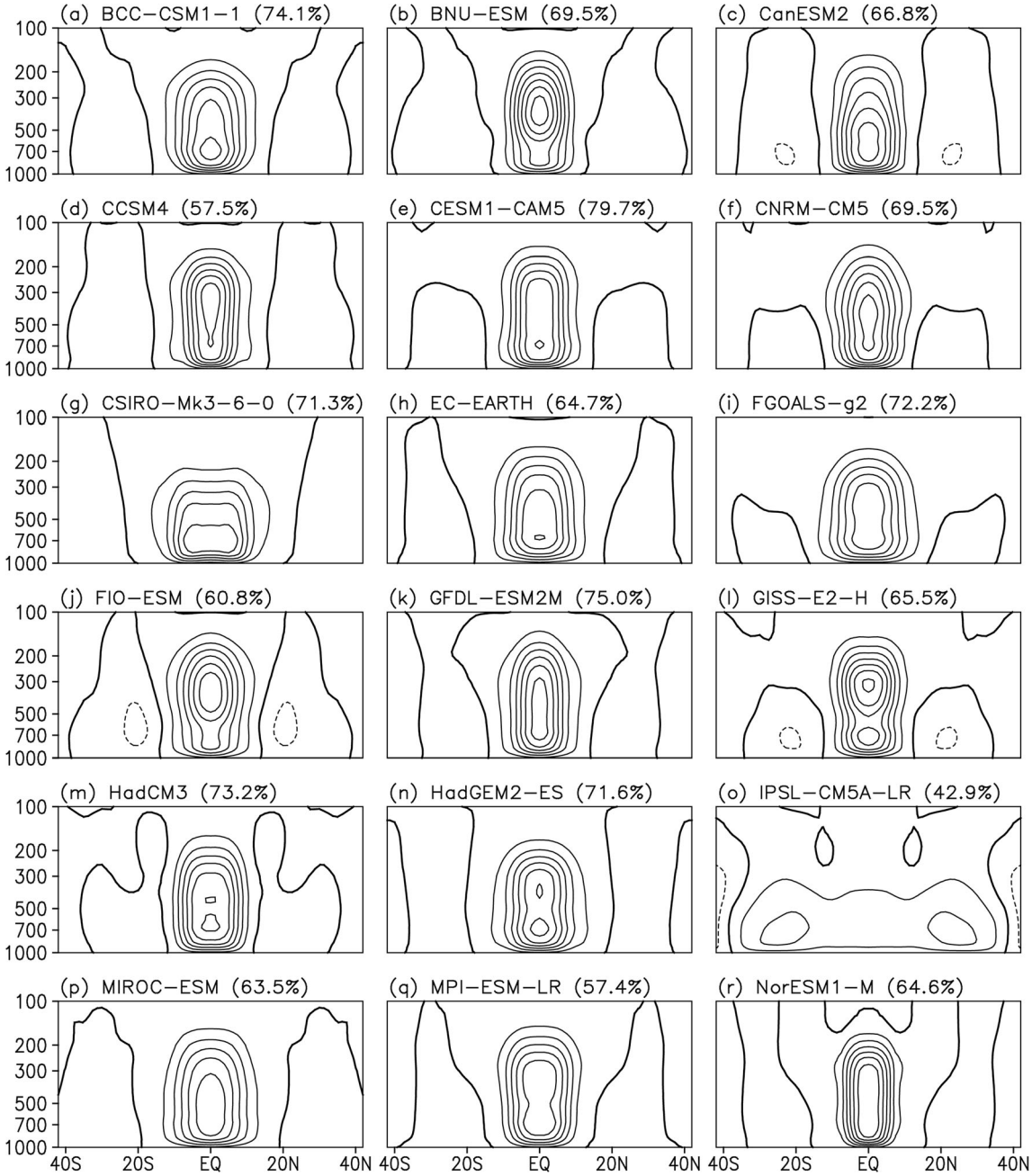

Fig. 4 **a**–**r** As in Fig. 3, but for the first principal mode of HEA in the CMIP5 models. The contour interval is 0.03×10^{10} kg/s

with the observations for the PCs of SES. The variations of SES corresponded to the symmetric variations of SST, which are associated with ENSO (Feng and Li 2013). This agrees with the findings of previous works, which also found that the simulation of ENSO variability is improved in the CMIP5 models (Guilyard et al. 2012; Kug et al. 2012; Bellenger et al. 2014; Bhaskar et al. 2014).

The differences in the responses of HEA to SEA and HES to SES are therefore assessed. Our results showed that only five models (BNU-ESM, CanESM2, CNRM-CM5, HadGEMs-ES, and HadCM3) displayed reasonable response differences between HEA to SEA and HES to SES. It should be noted that the CNRM_CM5, BCC_CSM1_1, and CANESM2 models showed a satisfactory performance in simulating the HC's long-term variability in Feng et al. (2015). The consistent results here highlight that the year-to-year variability of the HC and its relationship with SST are replicated well in these model simulations. Conversely, the response ratios of HEA to SEA and HES to SES are not constant and vary depending on the background climate. These models (i.e., CNRM_CM5, BCC_CSM1_1, and CANESM2) could therefore be used to further assess the

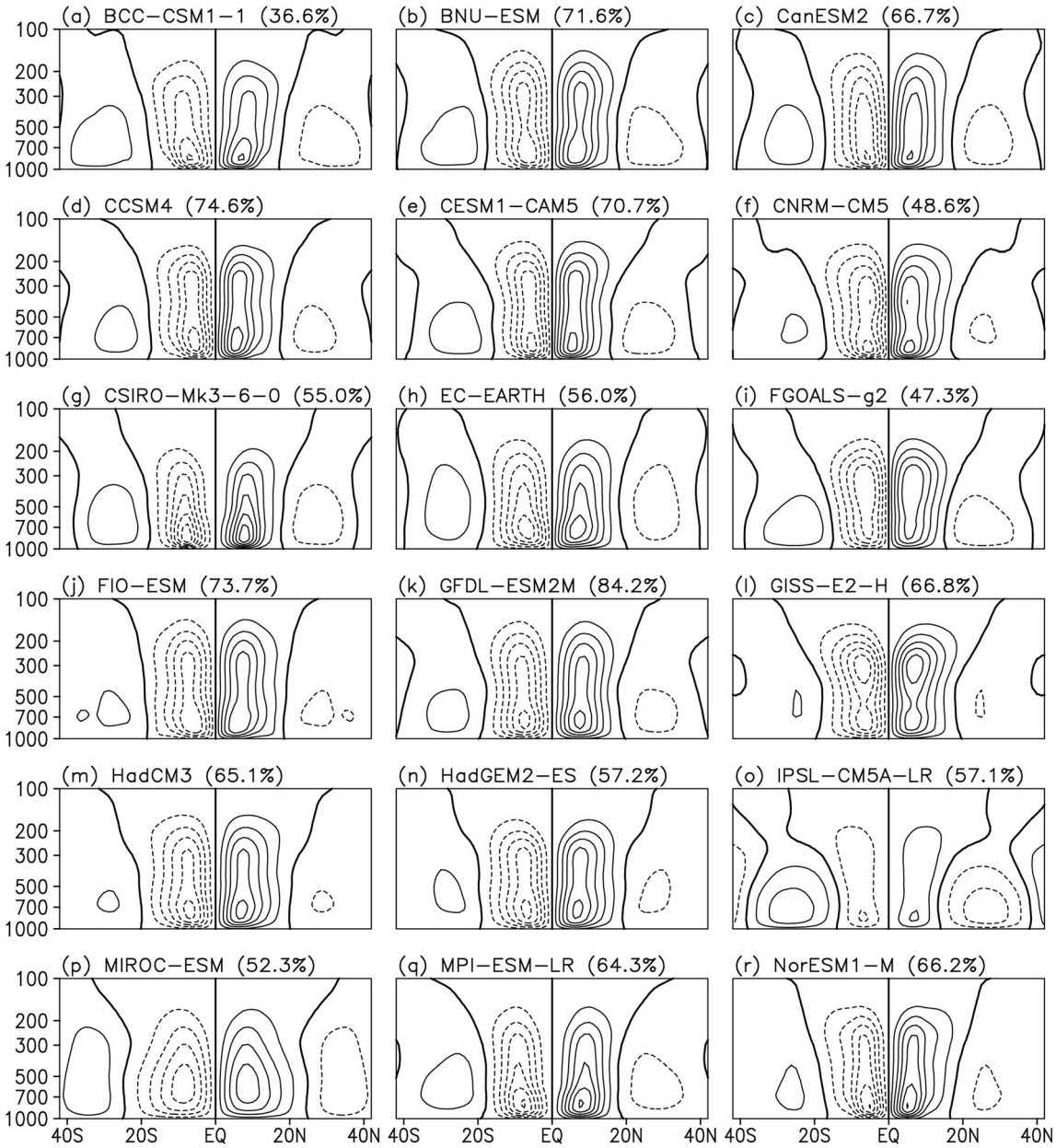

Fig. 5 As in Fig. 4, but for the HES

responses of HC to SST under different climatic backgrounds using their long historical outputs combined with future climatic scenarios (e.g., RCP8.5 and RCP4.5). This is out of the scope of this work, but could be a topic for future research.

On the other hand, the influence of SST on the HC involves complex linear and nonlinear processes, and SEA may also influence the variation of HES (Feng et al. 2016). However, the decomposition method here is linear, and that only the responses of HEA to SEA and HES to SES were discussed. This is due to the fact that the correlation coefficient of SEA (SES) and HES (HEA) is moderate (below or around 0.4 across different datasets) comparing to that of HEA to SEA and HES to SES, indicating the major influences of HES (HEA) are subject to SES (SEA). Hence, only the linear response of HC to SST was considered and assessed in the CMIP5 models. At present, we could not decompose the variations of HC and SST into linear and nonlinear components. The method described in this study provides a simple method to separately examine the possible linear impacts of SST on the HC.

Finally, the simulations of the response differences of HEA to SEA and HES to SES in the CMIP5 models vary greatly, indicating the presence of certain uncertainties within the models. The models capture the long-term variability of SES better than SEA (particularly the corresponding PCs), possibly because the variation of SEA reflects mainly the interdecadal

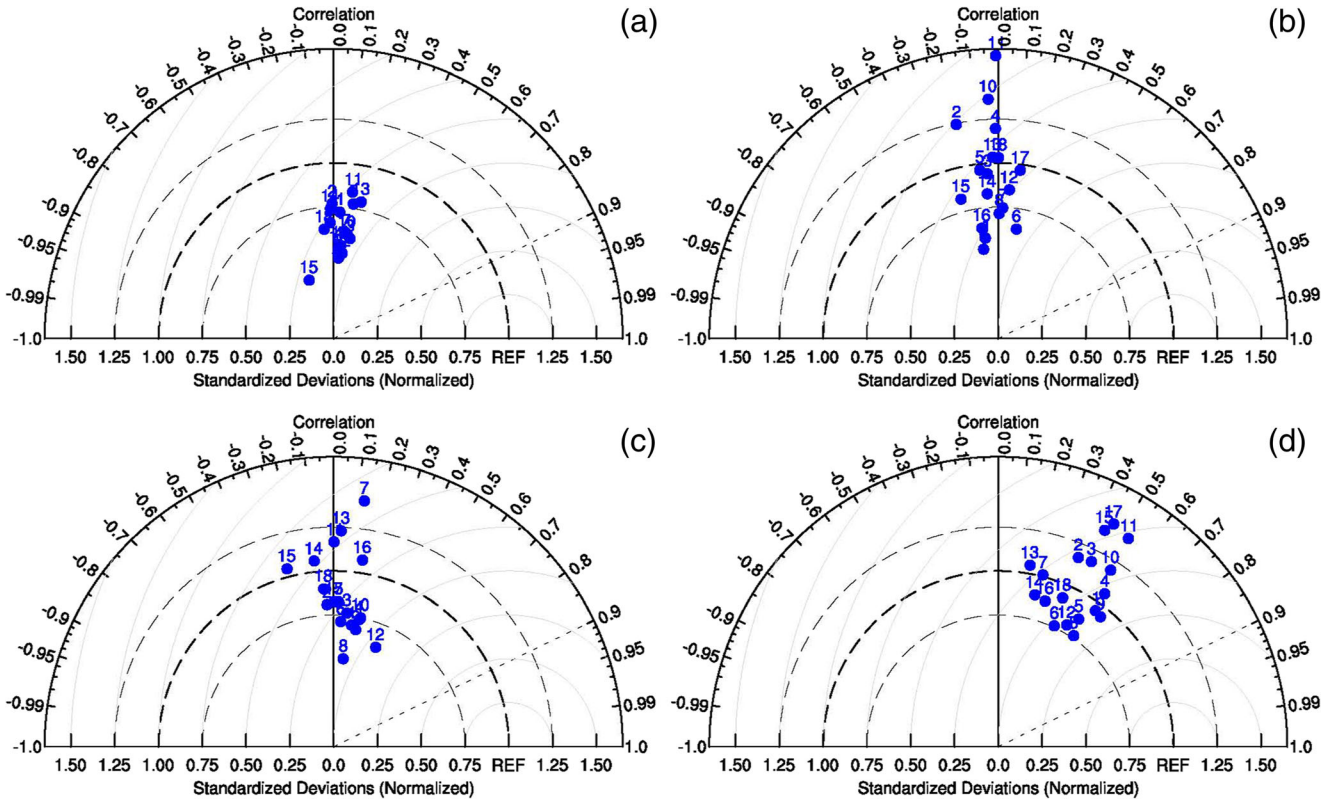

Fig. 6 As in Fig. 1, but for the Taylor diagram of the PCs between the observations and those in the models for **a** HEA, **b** HES, **c** SEA, and **d** SES. The solid circles (numbered) refer to the 18 models

variations of the HC, whereas HES represents mainly the interannual variations of the HC (Feng et al. 2016), and the variation of SES is closely linked with ENSO. This agrees with previous studies that reported the models do not simulate interdecadal variations well (e.g., Chiang et al. 2013; Yin et al. 2013; Zheng et al. 2013; Liu et al. 2016) and an improved ENSO simulated performance is found (Kug et al. 2012). Moreover, only the potential role of tropical SST on the HC is discussed in the context; however, both the tropical SST and HC may be influenced by many other climatic systems, such

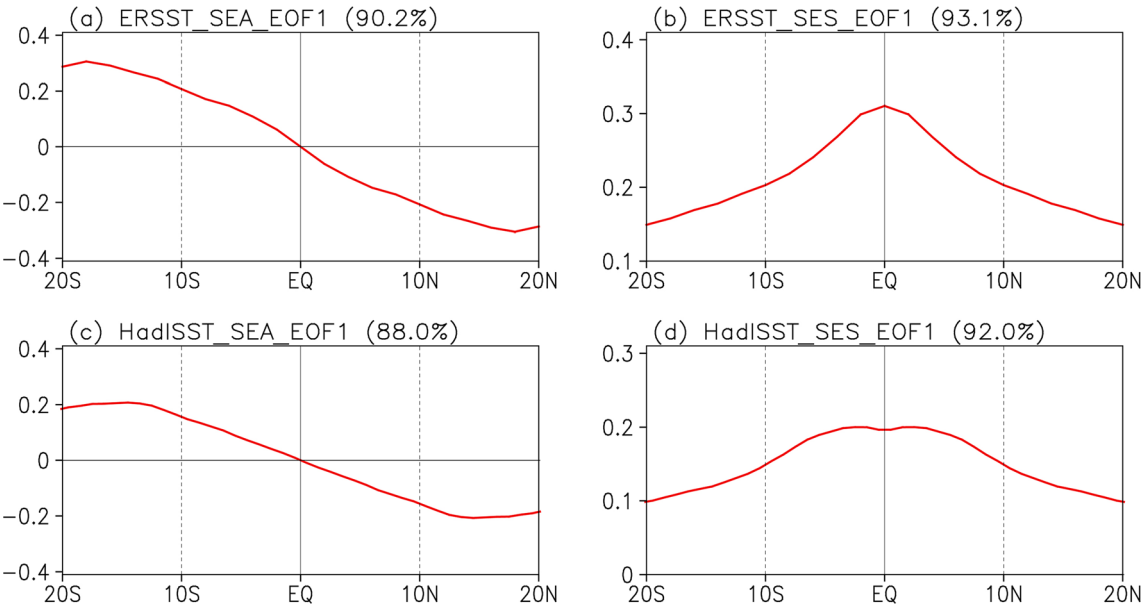

Fig. 7 **a** The first principal mode of SEA based on the ERSST. **b** As in (**a**), but for the SES. **c** As in (**a**), but based on the HadISST. **d** As in (**c**), but for the SES

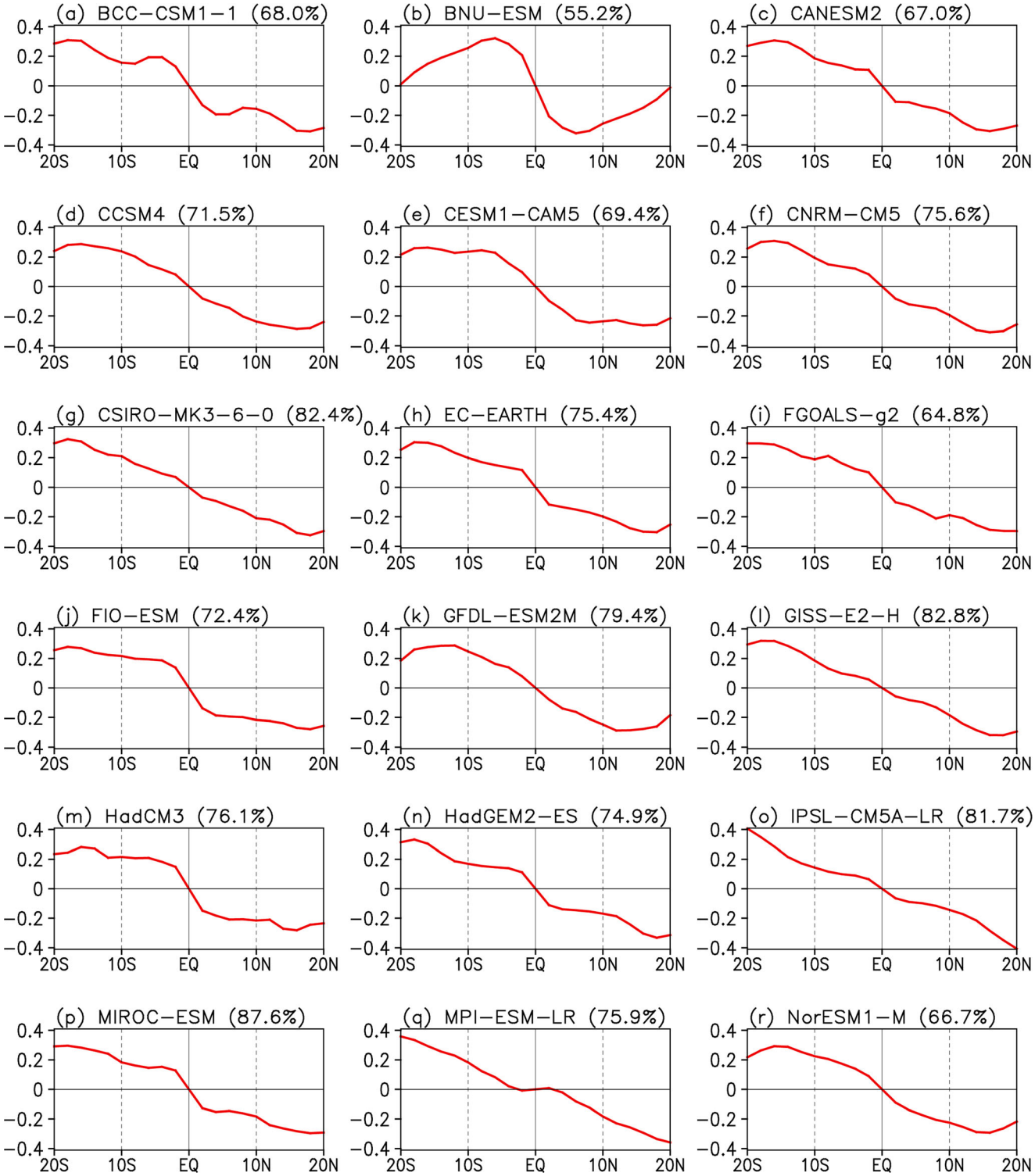

Fig. 8 The first principal mode of SEA in the CMIP5 models (°C)

as the Atlantic multi-decadal oscillation and the Antarctic oscillation (e.g., Zheng et al. 2015; Guo et al. 2016). However, neither the climatic effects nor the impacts of the variability of these large-scale oscillations have been reasonably reproduced by the models (e.g., Ruiz et al. 2013; Zheng et al. 2013; Han et al. 2016). This provides other plausible explanations why the response differences between the equatorially asymmetric and symmetric circulations to SST are not simulated well in the models, and warrant further researches. Nevertheless, we find that the response of the HC to

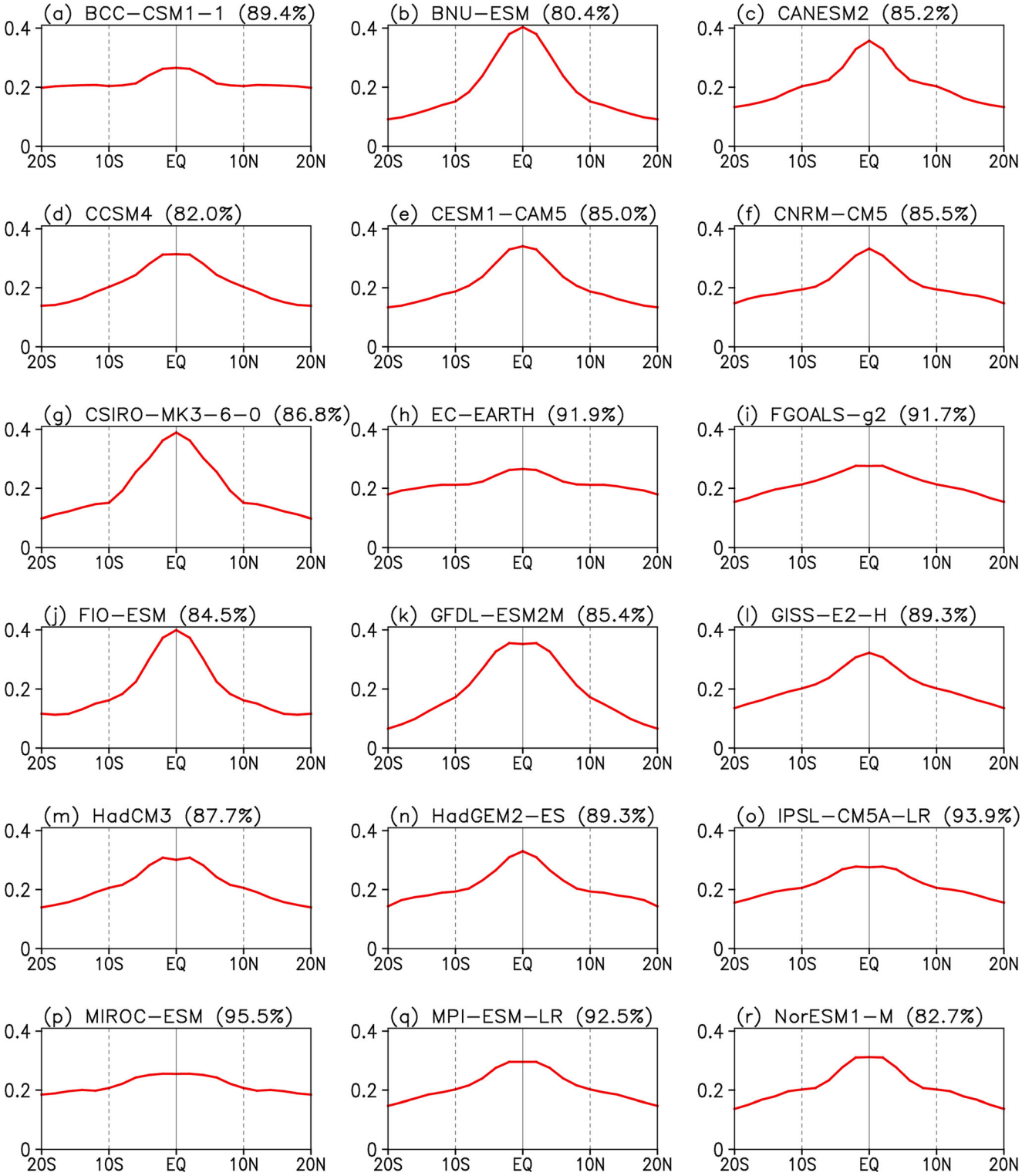

Fig. 9 As in Fig. 8, but for the SES (°C)

SST shows large uncertainties in the present models; this is due to the reason that both the long-term variabilities of SST and HC, particularly the temporal variations, are not well reproduced despite the limitations of the CMIP5 models and linear methodology used. The result provides a possible explanation why uncertainties exist in the long-term variability of HC in the current models, for the response of HC to tropical SST is not well reproduced. This may be due to the following aspects, unsatisfactory simulations in variability of tropical SST, and involved adjustment of the atmosphere to

the thermal structure and convergence process, implying an improvement in the relevant physical process involving the tropical air–sea interactions. This result may therefore contribute to the improvement of the CMIP5 models.

Acknowledgements This work was supported by the SOA Program on Global Change and Air–Sea interactions (GASI-IPOVAI-03) and National Natural Science Foundation of China (41475076). The HadISST dataset was obtained from the Met Office Hadley Centre and is available online at http://www.metoffice.gov.uk/hadobs/hadisst/data/download.html. The NCEP/NCAR reanalysis and ERSST were obtained from NOAA and are available at http://www.esrl.noaa.gov/psd/data/gridded/. We acknowledge the WCRP's Working Group on Coupled Modeling, which is responsible for CMIP5, and the climate modeling groups listed in Table 1 for their contribution to make the WCRP model output available.

References

Bellenger H, Guiyardi E, Leloup J, Lengaigne M, Vialard J (2014) ENSO representation in climate models: from CMIP3 to CMIP5. Clim Dyn 42(7-8):1999–2018. https://doi.org/10.1007/s00382-013-1783-z

Bentsen M, Bethke I, Debernard JB et al (2013) The Norwegian earth system model, NorESM1-M-part 1: description and basic evaluation of the physical climate. Geosci Model Dev 6(3):687–720. https://doi.org/10.5194/gmd-6-687-2013

Bhaskar J, Hu ZZ, Kumar A (2014) SST and ENSO variability and change simulated in historical experiments of CMIP5 models. Clim Dyn 42(7):2113–2124. https://doi.org/10.1007/s00382-013-1803-z

Chen G, Plumb RA, Lu J (2010) Sensitivities of zonal mean atmospheric circulation to SST warming in an aqua-planet model. Geophys Res Lett 37(12):L12701. https://doi.org/10.1029/2010GL043473

Chiang JC, Chang CY, Wehner MF (2013) Long-term behavior of the Atlantic interhemispheric SST gradient in the CMIP5 historical simulations. J Clim 26(21):8628–8640. https://doi.org/10.1175/JCLI-D-12-00487.1

Chylek P, Li J, Dubey MK, Wang M, Lesins G (2011) Observed and model simulated 20th century Arctic temperature variability: Canadian earth system model CanESM2. Atmos Chem Phys Discuss 11(8):22893–22907. https://doi.org/10.5194/acpd-11-22893-2011

Clement AC (2006) The role of the ocean in the seasonal cycle of the Hadley circulation. J Atmos Sci 63(12):3351–3365. https://doi.org/10.1175/JAS3811.1

Collier MA, Jeffrey SJ, Rotstayn LD, et al. (2011) The CSIRO-Mk3.6.0 Atmosphere–Ocean GCM: participation in CMIP5 and data publication. 19th International Congress on Modelling and Simulation, Perth, Australia, 12–16 December 2011. http://mssanz.org.au/modsim2011

Compo GP, Whitaker JS, Sardeshmukh PD, Matsui N, Allan RJ, Yin X, Gleason BE, Vose RS, Rutledge G, Bessemoulin P, Brönnimann S, Brunet M, Crouthamel RI, Grant AN, Groisman PY, Jones PD, Kruk MC, Kruger AC, Marshall GJ, Maugeri M, Mok HY, Nordli Ø, Ross TF, Trigo RM, Wang XL, Woodruff SD, Worley SJ (2011) The twentieth century reanalysis project. Q J R Meteorol Soc 137(654):1–28. https://doi.org/10.1002/qj.776

Dufresne JL, Foujols MA, Denvil S, Caubel A, Marti O, Aumont O, Balkanski Y, Bekki S, Bellenger H, Benshila R, Bony S, Bopp L, Braconnot P, Brockmann P, Cadule P, Cheruy F, Codron F, Cozic A, Cugnet D, de Noblet N, Duvel JP, Ethé C, Fairhead L, Fichefet T, Flavoni S, Friedlingstein P, Grandpeix JY, Guez L, Guilyardi E, Hauglustaine D, Hourdin F, Idelkadi A, Ghattas J, Joussaume S, Kageyama M, Krinner G, Labetoulle S, Lahellec A, Lefebvre MP, Lefevre F, Levy C, Li ZX, Lloyd J, Lott F, Madec G, Mancip M, Marchand M, Masson S, Meurdesoif Y, Mignot J, Musat I, Parouty S, Polcher J, Rio C, Schulz M, Swingedouw D, Szopa S, Talandier C, Terray P, Viovy N, Vuichard N (2013) Climate change projections using the IPSL-CM5 earth system model: from CMIP3 to CMIP5. Clim Dyn 40(9):2123–2165. https://doi.org/10.1007/s00382-012-1636-1

Dunne JP, John JG, Shevliakova E, Stouffer RJ, Krasting JP, Malyshev SL, Milly PCD, Sentman LT, Adcroft AJ, Cooke W, Dunne KA, Griffies SM, Hallberg RW, Harrison MJ, Levy H, Wittenberg AT, Phillips PJ, Zadeh N (2013) GFDL's ESM2 global coupled climate–carbon earth system models. Part II: carbon system formulation and baseline simulation characteristics. J Clim 26(7):2247–2267. https://doi.org/10.1175/JCLI-D-12-00150.1

Feng J, Li JP (2013) Contrasting impacts of two types of ENSO on the boreal spring Hadley circulation. J Clim 26(13):4773–4789. https://doi.org/10.1175/JCLI-D-12-00298.1

Feng R, Li JP, Wang JC (2011) Regime change of the boreal summer Hadley circulation and its connection with the tropical SST. J Clim 24(15):3867–3877. https://doi.org/10.1175/2011JCLI3959.1

Feng J, Li JP, Xie F (2013) Long-term variation of the principal mode of boreal spring Hadley circulation linked to SST over the Indo-Pacific warm pool. J Clim 26(2):532–544. https://doi.org/10.1175/JCLI-D-12-00066.1

Feng J, Li JP, Zhu JL et al (2015) Simulation of the equatorially asymmetric mode of the Hadley circulation in CMIP5 models. Adv Atmos Sci 32(8):1129–1142. https://doi.org/10.1007/s00376-015-4157-0

Feng J, Li JP, Jin FF et al (2016) Contrasting responses of the Hadley circulation to equatorially asymmetric and symmetric meridional sea surface temperature structures. J Clim 29(24):8949–8963. https://doi.org/10.1175/JCLI-D-16-0171.1

Feng J, Li JP, Jin FF et al (2017) The responses of the Hadley circulation to different meridional SST structures in the seasonal cycle. J Geophys Res Atmos 122(15):7785–7789. https://doi.org/10.1002/2017JD026953

Gastineau G, Treut HL, Li L (2008) Hadley circulation changes under global warming conditions indicated by coupled climate modes. Tellus 60A(5):863–884. https://doi.org/10.1111/j.1600-0870.2008.00344.x

Gent PR, Danabasoglu G, Donner LJ et al (2011) The community climate system model version 4. J Clim 24(19):4973–4991. https://doi.org/10.1175/2011JCLI4083.1

Giorgetta MA, Jungclaus J, Reick CH, Legutke S, Bader J, Böttinger M, Brovkin V, Crueger T, Esch M, Fieg K, Glushak K, Gayler V, Haak H, Hollweg HD, Ilyina T, Kinne S, Kornblueh L, Matei D, Mauritsen T, Mikolajewicz U, Mueller W, Notz D, Pithan F, Raddatz T, Rast S, Redler R, Roeckner E, Schmidt H, Schnur R, Segschneider J, Six KD, Stockhause M, Timmreck C, Wegner J, Widmann H, Wieners KH, Claussen M, Marotzke J, Stevens B (2013) Climate and carbon cycle changes from 1850 to 2100 in MPI-ESM simulations for the coupled model Intercomparison project phase 5. J Adv Model Earth Syst 5(3):572–597. https://doi.org/10.1002/jame.20038

Gordon C, Cooper C, Senior CA et al (2000) The simulation of SST, sea ice extents and ocean heat transports in a version of the Hadley Centre coupled model without flux adjustments. Clim Dyn 16(2-3):147–168. https://doi.org/10.1007/s003820050010

Guilyard E, Bellenger H, Collins M et al (2012) A first look at ENSO in CMIP5. CLIVAR Exchange 17(1):29–32

Guo YP, Li JP, Feng J et al (2016) The multidecadal variability of the asymmetric mode of the boreal autumn Hadley circulation and its

link to the Atlantic multidecadal oscillation. J Clim 29(15):5625–5641. https://doi.org/10.1175/JCLI-D-15-0025.1

Han Z, Luo FF, Li SL et al (2016) Simulation by CMIP5 models of the Atlantic multidecadal oscillation and its climate impacts. Adv Atmos Sci 33(12):1329–1342. https://doi.org/10.1007/s00376-016-5270-4

Hazeleger W, Wang X, Severijns C et al (2011) EC-ERATH V2.2: description and validation of a new seamless earth system prediction model. Clim Dyn 39(11):1–19. https://doi.org/10.1007/s00382-011-1228-5

Hou AY, Lindzen RS (1992) The influence of concentrated heating on the Hadley circulation. J Atmos Sci 49(14):1233–1241. https://doi.org/10.1175/1520-0469(1992)049

Hu YY, Tao LJ, Liu JP (2013) Poleward expansion of the Hadley circulation in CMIP5 simulations. Adv Atmos Sci 30(3):790–795. https://doi.org/10.1007/s00376-01202187-4

Ji DY, Wang LN, Feng J et al (2014) Description and basic evaluation of BNU-ESM version 1. Geosci Model Dev Discuss 7(5):1601–1647. https://doi.org/10.5194/gmd-7-2039-2014

Jiang Y, Luo Y, Zhao ZC (2010) Projection of wind speed changes in China in the 21st century by climate models. Chin J Atmos Sci 34: 323–336

Kalnay E, Kanamitsu M, Kilster R et al (1996) The NCEP/NCAR 40-year reanalysis project. Bull Am Meteorol Soc 77:437–472. https://doi.org/10.1175/1520-0477(1996)077

Kug JS, Ham YG, Lee JY, Jin FF (2012) Improved simulation of two types of El Niño in CMIP5 models. Environ Res Lett 7(3):034002. https://doi.org/10.1088/1748-9326/7/3/034002

Li JP, Feng J (2017) Tropical large-scale atmospheric interaction in association with subtropical aridity trend. Fu CB, Mao HT (eds) Aridity trend in Northern China. World Scientific Publishing Co Pte Ltd, Singapore, pp 320

Lindzen RS, Nigam S (1987) On the role of sea surface temperature gradients in forcing low-level winds and convergence in the tropics. J Atmos Sci 44(17):2418–2436. https://doi.org/10.1175/1520-0469(1987)044<2418:OTROSS>2.0.CO;2

Liu T, Li JP, Feng J et al (2016) Cross-seasonal relationship between the boreal autumn SAM and winter precipitation in the Northern Hemisphere in CMIP5. J Clim 29(18):6617–6636. https://doi.org/10.1175/JCLI-D-15-0708.1

Ma J, Li JP (2007) The reason for the strengthening of the boreal winter Hadley circulation and its connection with ENSO. Prog Nat Sci 17(11):1327–1333

Ma J, Li JP (2008) The principal modes of variability of the boreal winter Hadley cell. Geophys Res Lett 35(1):L01808. https://doi.org/10.1029/2007GL031883

Martin GM, Bellouin N, Collins WJ et al (2011) The HadGEM2 family of Met Office unified model climate configurations. Geosci Model Dev 4(3):723–757. https://doi.org/10.5194/gmd-4-723-2011

Mitas CM, Clement A (2005) Has the Hadley cell been strengthening in recent 329 decades? Goephys Res Lett 32(3):L03809. https://doi.org/10.1029/2004GL021765

Mitas CM, Clement A (2006) Recent behavior of the Hadley cell and tropical thermodynamics in climate models and reanalyses. Geophys Res Lett 33(1):L01810. https://doi.org/10.1029/2005GL024406

Neale RB, Chen CC, Gettelman A, et al. (2012) Description of the NCAR Community Atmospheric Model (CAM5.0). NCAR TECHNICAL NOTE, NCAR/TN-486+STR, http://www.cesm.ucar.edu/models/cesm1.0/cam/docs/description/cam5_desc.pdf

Oort AH, Yienger JJ (1996) Observed interannual variability in the Hadley circulation and its connection to ENSO. J Clim 9(11): 2751–2767. https://doi.org/10.1175/1520-0442(1996)009

Qiao FL, Song ZY, Bao Y et al (2013) Development and evaluation of an earth system model with surface gravity waves. J Geophys Res 118(9):4514–4524. https://doi.org/10.1002/jgrc.20327

Rayner NA, Parker D, Horton E, et al. (2003) Global analyses of sea surface temperature, sea ice, and night marine air temperature since the late nineteenth century. J Geophys Res 108. doi:https://doi.org/10.1029/2002JD002670, D14

Rind D, Rossow WB (1984) The effects of physical processes on the Hadley circulation. J Atmos Sci 41(4):479–507. https://doi.org/10.1175/1520-0469(1984)041

Ruiz BA, Nigam S, Kavvada A (2013) The Atlantic multidecadal oscillation in twentieth century climate simulations: uneven progress from CMIP3 to CMIP5. Clim Dyn 41(11-12):3301–3315. https://doi.org/10.1007/s00382-013-1810-0

Schmidt GA, Kelley M, Nazarenko L, Ruedy R, Russell GL, Aleinov I, Bauer M, Bauer SE, Bhat MK, Bleck R, Canuto V, Chen YH, Cheng Y, Clune TL, del Genio A, de Fainchtein R, Faluvegi G, Hansen JE, Healy RJ, Kiang NY, Koch D, Lacis AA, LeGrande AN, Lerner J, Lo KK, Matthews EE, Menon S, Miller RL, Oinas V, Oloso AO, Perlwitz JP, Puma MJ, Putman WM, Rind D, Romanou A, Sato M, Shindell DT, Sun S, Syed RA, Tausnev N, Tsigaridis K, Unger N, Voulgarakis A, Yao MS, Zhang J (2014) Configuration and assessment of the GISS ModelE2 contributions to the CMIP5 archive. J Adv Model Earth Syst 6(1):141–184. https://doi.org/10.1002/2013MS000265

Schneider E, Lindzen RS (1977) Axially symmetric steady state models of the basic state of instability and climate studies. Part I: Linearized calculations. J Atmos Sci 34:253–279. https://doi.org/10.1175/1520-0469(1977)034

Smith TM, Reynolds RW, Peterson TC, Lawrimore J (2008) Improvements to NOAA's historical merged land–ocean surface temperature analysis (1880–2006). J Clim 21(10):2283–2296. https://doi.org/10.1175/2007JCLI2100.1

Sun Y, Zhou TJ (2014) How does El Niño affect the interannual variability of the boreal summer Hadley circulation? J Clim 27(7):2622–2642. https://doi.org/10.1175/JCLI-D-13-00277.1

Tanaka HL, Ishizaki N, Kitoh A (2004) Trend and interannual variability of Walker, monsoon and Hadley circulations defined by velocity potential in the upper troposphere. Tellus 56A(3):250–269. https://doi.org/10.1111/j.1600-0870.2004.00049.x

Taylor KE, Stouffer RJ, Meehl GA (2012) An overview of CMIP5 and the experiment design. Bull Am Meteorol Soc 93(4):485–498. https://doi.org/10.1175/BAMS-D-11-00094.1

Vecchi GA, Soden BJ (2007) Global warming and the weakening of the tropical circulation. J Clim 20(17):4316–4340. https://doi.org/10.1175/JCLI4258.1

Voldoire A et al (2013) The CNRM-CM5.1 global climate model: description and basic evaluation. Clim Dyn 40(9-10):2091–2121. https://doi.org/10.1007/s00382-011-1259-y

Watanabe S et al (2011) MIROC-ESM 2010: model description and basic results of CMIP5-20c3m experiments. Geosci Model Dev 4(4):845–872. https://doi.org/10.5194/gmd-4-845-2011

Yin L, Fu R, Shevliakova E, Dickinson RE (2013) How well can CMIP5 simulate precipitation and its controlling processes over tropical South America? Clim Dyn 41(11-12):3127–3143. https://doi.org/10.1007/s00382-012-1582-y

Yu YQ, Zheng WP, Wang B et al (2011) Versions g1.0 and g1.1 of the LASG/IAP flexible Global Ocean–Atmosphere–Land System model. Adv Atmos Sci 28(1):99–117. https://doi.org/10.1007/s00376-010-9112-5

Zhang WJ, Li JP, Jin FF (2009) Spatial and temporal features of ENSO meridional scales. Geophys Res Lett 36(15):L15605. https://doi.org/10.1029/2009GL038672

Zheng F, Li JP, Clark R, Nnamchi H (2013) Simulation and projection of the southern hemisphere annular mode in CMIP5 models. J Clim 26(24):9860–9879. https://doi.org/10.1175/JCLI-D-13-00204.1

Zheng F, Li JP, Wang L et al (2015) Cross-seasonal influence of the December–February southern hemisphere annular mode on March–May meridional circulation and precipitation. J Clim 28(17):6859–6881. https://doi.org/10.1175/JCLI-D-14-00515.1